Defect Tolerant Semiconductors for Solar Energy Conversion

ARTICLE *in* JOURNAL OF PHYSICAL CHEMISTRY LETTERS · MARCH 2014

Impact Factor: 7.46 · DOI: 10.1021/jz5001787

8 AUTHORS, INCLUDING:

Andriy Zakutayev
National Renewable Energy Laboratory
77 PUBLICATIONS **632** CITATIONS
SEE PROFILE

David S Ginley
National Renewable Energy Laboratory
608 PUBLICATIONS **13,809** CITATIONS
SEE PROFILE

Julien Vidal
Électricité de France (EDF)
35 PUBLICATIONS **506** CITATIONS
SEE PROFILE

Vladan Stevanovic
Colorado School of Mines
45 PUBLICATIONS **253** CITATIONS
SEE PROFILE

THE JOURNAL OF PHYSICAL CHEMISTRY Letters

Perspective

pubs.acs.org/JPCL

Defect Tolerant Semiconductors for Solar Energy Conversion

Andriy Zakutayev,*[,†] Christopher M. Caskey,[†,‡] Angela N. Fioretti,[†,‡] David S. Ginley,[†] Julien Vidal,[§] Vladan Stevanovic,[†,‡] Eric Tea,[§] and Stephan Lany[†]

[†]National Renewable Energy Laboratory, Golden, Colorado 80401, United States

[‡]Colorado School of Mines, Golden, Colorado 80401, United States

[§]Institute for Research and Development of Photovoltaic Energy (IRDEP), Chatou 78401, France

ABSTRACT: Defect tolerance is the tendency of a semiconductor to keep its properties despite the presence of crystallographic defects. Scientific understanding of the origin of defect tolerance is currently missing. Here we show that semiconductors with antibonding states at the top of the valence band are likely to be tolerant to defects. Theoretical calculations demonstrate that Cu_3N with antibonding valence band maximum has shallow intrinsic defects and no surface states, in contrast to GaN with bonding valence band maximum. Experimental measurements indicate shallow native donors and acceptors in Cu_3N thin films, leading to 10^{16}–10^{17} cm^{-3} doping with either electrons or holes depending on the growth conditions. The experimentally measured bipolar doping and the solar-matched optical absorption onset (1.4 eV) make Cu_3N a promising candidate absorber for photovoltaic and photoelectrochemical solar cells, despite the calculated indirect fundamental band gap (1.0 eV). These conclusions can be extended to other materials with antibonding character of the valence band, defining a class of defect-tolerant semiconductors for solar energy conversion applications.

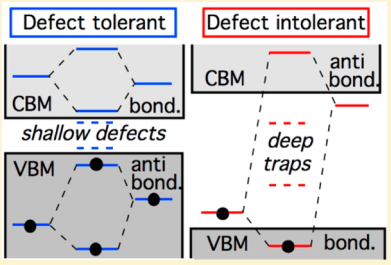

Defect-tolerant solar absorbers are semiconductors where the optoelectronic energy conversion efficiency is relatively insensitive to imperfections, such as point defects, dislocation, stacking faults, grain boundaries, and surfaces. An example of a defect tolerant absorber is $Cu(In,Ga)Se_2$ semiconductor alloy (CIGS), which can have >20% photovoltaic performance despite rough polycrystalline morphology, percent range off-stoichiometry, and nonstoichiometric grain boundaries.[1] The CIGS solar cells can be prepared by various techniques ranging from vacuum to wet processing, making this technology amenable to commercialization. This contrasts with the need for using specialized MBE or MOCVD techniques for fabrication of high efficiency multijunction solar cells.[2] The constituent III–V semiconductors (e.g., GaAs, GaN) are notorious for intolerance of optoelectronic device performance to point defects, stacking faults, threading dislocations, surfaces and other imperfections. Understanding the scientific origin of this dramatic difference is important for designing new defect tolerant semiconductors for next-generation Earth-abundant solar energy conversion,[3] including photovoltaic (PV)[4] and photoelectrochemical (PEC)[5] solar cells.

One of the possible origins of defect tolerance in semiconductors is the electronic structure with the antibonding character of the valence band maximum (VBM) and bonding character of the conduction band minimum (CBM), as shown in the Abstract graphic. Note that this unusual electronic structure order (antibonding VBM and bonding CBM) is opposite to that of the majority of the semiconducting materials (bonding VBM and antibonding CBM). In such unusual semiconductors, the electronic energy levels of the constituent elements are resonant with the valence and conduction bands, so the defect states that result from removal/insertion of these elements into the crystal structure fall into the bands rather than in the band gap, and lead to effective-mass-like shallow states close to the band edges rather than deep defects states in the gap. The resulting minimal scattering of electrons and holes contrasts with deep carrier traps in conventional semiconductors. This defect tolerance electronic structure argument can be extended beyond vacancies and interstitials to other defects such as antisites, surfaces, and dislocation, because bond breaking underpins formation of these defects just like in the case of the simple point defects. Other possible origins of defect tolerance, for example, the chalcopyrite crystal structure, are less likely because II–IV–V_2 chalcopyrites,[6] such as $ZnSnN_2$[7] and $ZnSnP_2$,[8] appear from the literature to be more sensitive to defects than the I–III–VI_2 chalcopyrites, such as $CuInSe_2$ and $CuGaSe_2$.

> Defect tolerance is the tendency of a semiconductor to keep its properties despite the presence of crystallographic defects.

In this work, we show how electronic structure of a semiconductor can lead to its defect tolerance and result in optoelectronic properties that are favorable for solar energy conversion applications. First, we support the electronic structure origin of defect tolerance by a comparative computa-

Received: January 26, 2014
Accepted: March 13, 2014
Published: March 13, 2014

   dx.doi.org/10.1021/jz5001787 | *J. Phys. Chem. Lett.* 2014, 5, 1117–1125

tional study of two model semiconductors, Cu_3N and GaN. We find that tolerance of Cu_3N to bulk and surface defects originates from its antibonding valence band and bonding conduction band, and contrast these observations with GaN. Next, we perform the experiments to support these theoretical findings and to demonstrate the implication of this peculiar electronic structure to solar energy conversion potential of Cu_3N. Our experiments indicate that Cu_3N thin films can be doped both *p*-type and *n*-type, and that Cu_3N has 1.4 eV optical absorption onset, while the calculated indirect band gap is 1.0 eV. Finally, we discuss how surface passivation and long-term stability of Cu_3N are important to its potential photovoltaic applications. Overall, our studies suggest that copper nitrides, including the binary Cu_3N and related ternaries, are a promising design space for Earth-abundant defect tolerant semiconductors for solar energy conversion applications.

Semiconductors with antibonding states at the top of the valence band are likely to be tolerant to defects.

Model Materials. The two model materials considered in the theoretical part of this work are Cu_3N and GaN (Figure 1). The

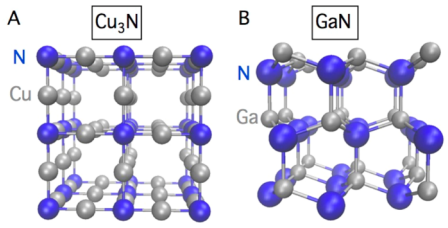

Figure 1. Crystal structures of (a) Cu_3N with 2-fold coordinated Cu atoms and 8-fold coordinated N atoms, and (b) GaN with 4-fold coordinated atoms. In both pictures, small blue spheres indicate nitrogen atoms, and the gray spheres indicate metal atoms.

GaN and related III–V binary compounds (GaAs, InP) have tetrahedrally bonded crystal structures (Figure 1b) and bonding valence band maxima. For decades the GaN and related materials have been studied for their applications in various optoelectronic devices, including light-emitting diodes,[9] and solar cells.[10] The Cu_3N and related Cu(+I)-based materials such as Cu_2O,[11] and $CuAlO_2$,[12,13] feature 2-fold coordinated Cu atoms (Figure 1a) and usually have antibonding VBM. Recently, Cu-based oxides, sulfides,[14,15] and mixed-anion compounds[16,17] have attracted a lot of attention as photovoltaic[18,19] and photoelectrochemical[20,21] absorbers, thermoelectrics,[22,23] transparent conductors,[24,25] and channel layers in transparent transistors.[26,27] Much less is known about semiconductor related applications of Cu_3N material, although possible synthetic routes,[28,29] basic electronic structure,[30,31] some physical properties,[32,33] and potential nonsemiconductor applications[34,35] have been reported. Below we compare bulk electronic structures, surface features, and point defect properties of Cu_3N and GaN, and discuss the connection of these theoretical results to defect tolerance.

Electronic Structure. As anticipated in the Abstract graphic, the atom- and symmetry-projected density of states (DOS) reveals a strong *p*–*d* interaction in the valence band of Cu_3N, akin to that in $CuInSe_2$ chalcopyrite. Pronounced Cu-*d*/N-*p* bonding and antibonding interactions occur in the valence band as resonances in the DOS at −6 and −12 eV, respectively (Figure 2b). In contrast, the valence band of GaN is almost exclusively

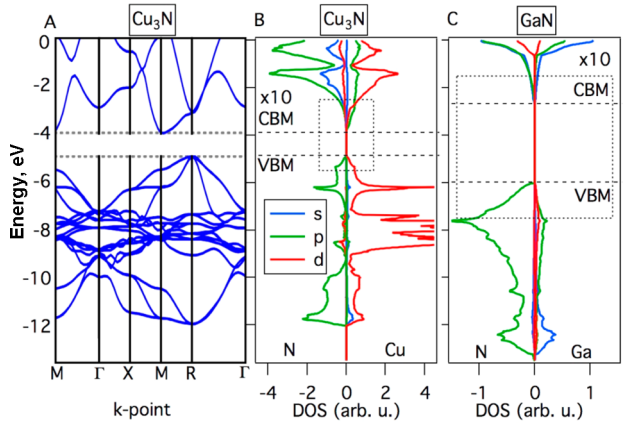

Figure 2. The band structure of Cu_3N (a) and partial DOS of (b) Cu_3N and (c) GaN determined from GW quasiparticle energy calculations. Consistent with the Abstract graphic, the VBM and CBM of Cu_3N have mixed Cu–N character (b), whereas GaN features mostly N-derived VBM and Ga-derived CBM (c). The origin of the vertical axis in a, b, and c aligns with the vacuum level calculated in Figure 3, and dotted squares in b and c indicate the range of the corresponding surface plots in Figure 3.

composed of N-*p* states with a strong resonance at −7.5 eV (Figure 2c). The Ga-*s* state at −13 eV is indicative of the covalent Ga-*s*/N-*p* bonding interaction, which is typical for *s*–*p* bonded compound semiconductors. The respective empty Ga-*s* state forms the highly dispersive conduction band of GaN. Notably, the empty N-3*s* and N-3*p* atomic states also provide a considerable contribution to the conduction band DOS (Figure 2b). However, in the conduction band of Cu_3N (Figure 2b), there are additional interactions that do not exist in GaN: a strong component due to Cu-*d* states, which result from the 2-fold coordinated N–Cu–N dumbbell structure that allows on-site *s*-*d* hybridization, as well as Cu-4*p* derived states that mix into the conduction band of Cu_3N over a wide energy range. In the past, the Cu states with *s* and *p* character have been also shown to be essential for the partially covalent bonding character of Cu_3N and related materials with dumbbell coordinated Cu atoms.[30] These additional contributions cause a larger width of the conduction band, smaller band gap, and a larger electron affinity than in GaN, as schematically indicated in the Abstract graphic.

The band structure of Cu_3N from the GW quasiparticle energy calculations is shown in Figure 2a, and the band-structure properties are summarized in Table 1. According to GW band structure calculations, Cu_3N is an indirect band gap semiconductor with 1.0 eV band gap between VBM at the R point and CBM at the M-point. The first direct transition is 1.6 eV at the M-point of *k*-space, in qualitative agreement with previously published Cu_3N band structure calculated in the local density approximation.[30] Despite the difference in the electronic structures, the electron and hole effective masses of Cu_3N a GaN calculated from their density of states are similar, but in the case of Cu_3N (Figure 2a), they appear somewhat anisotropic. More calculation details are provided in the Methods section.

dx.doi.org/10.1021/jz5001787 | J. Phys. Chem. Lett. 2014, 5, 1117–1125

Table 1. Band-Structure Properties of Cu_3N and GaN from the GW Quasiparticle Energy Calculations[a]

material	Cu_3N	GaN
VBM	R	Γ
CBM	M	Γ
E_g (eV)	1.0	3.5
E_g^{dir} (eV)	1.5	3.5
m_h^* (m_0)	2.3	2.2
m_e^* (m_0)	0.5	0.2
IP (eV)	4.9	6.8

[a]The Brillouin zone locations of the VBM and the CBM, the lowest energy band gap E_g, the direct band gap E_g^{dir}, the average hole and electron density of states effective masses m_h^* and m_e^*, and the ionization potential (IP) for the O-passivated (100) Cu_3N and for the $(10\bar{1}0)$ GaN surface.

Theoretical calculations demonstrate that Cu_3N with an antibonding valence band maximum has shallow intrinsic defects and no surface states, in contrast to GaN.

Surfaces. The theoretical evaluation of bare Cu_3N surfaces is difficult because of their polar and off-stoichiometric character, but experiments described below indicate that unprotected (001) Cu_3N surfaces are covered with a native oxide. On the basis of this experimental insight, a nonpolar (001) Cu_3N surface slab is constructed, where the excess charge due to a N-rich surface composition is compensated by replacing 1/2 of the surface N ions by O, such that the local dumbbell coordination of Cu, as present in both Cu_3N and Cu_2O, is maintained (Figure 3a). The calculated surface energy for a $\sqrt{2}$ x $\sqrt{2}$ surface unit cell is 29 meV/Å^2, compared to 35 meV/Å^2 for the 2 × 1 reconstruction. These surface energies are significantly lower compared to 96 and 102 meV/Å^2 for $(10\bar{1}0)$ and $(11\bar{2}0)$ low energy nonpolar GaN surfaces respectively. This extremely low surface energy indicates a high stability of the O-passivated Cu_3N (001) surface, suggesting that our structural model provides a realistic description of the situation. In contrast, hypothetical unpassivated Cu_3N surfaces have higher surface energies either due to excess charges resulting from off-stoichiometric surface compositions or due to containing singly coordinated Cu ad-atoms.

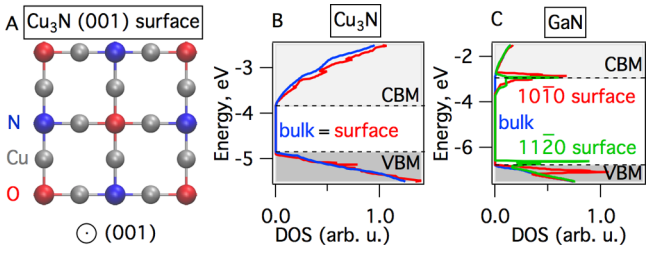

Figure 3. The model of the calculated oxygen passivated Cu_3N surface (a). Total density of states of bulk and surface electronic structure of (b) polar Cu_3N (001) surface passivated with oxygen, and (c) two different nonpolar GaN surfaces. The GaN surfaces show trap states (c), whereas the Cu_3N surface does not (b), supporting the defect tolerance argument demonstrated in Abstract graphic. The origin of the energy scale in both b and c aligns with the vacuum level.

Using this surface model for Cu_3N (Figure 3a), we calculated the band lineup with respect to the vacuum level and the surface electronic structure. As summarized in Table 1, the calculated ionization potential of the oxygen-passivated Cu_3N surface (4.9 eV) is much smaller than that of GaN surfaces (6.8 eV), reflecting the antibonding character of the VBM of Cu_3N (see Abstract graphic). As seen in Figure 3b, the calculated Cu_3N (001) oxygen passivated surface shows no electronic states inside the band gap. This contrasts with the low-energy GaN surfaces that show sharp peaks close to the band edges (Figure 3c). Similar surface states have been found in previous calculations for both wide-gap GaN and narrow-gap InN,[36] and more recently experimentally confirmed in GaN.[37] While the effect of such surface states can be mitigated by specific passivation strategies,[38,39] their presence is a sign of defect-intolerance, since it implies that charge carriers become trapped at the surface, often followed by localization in a gap state. The propensity of a material to form such states at the surface further suggests that similar states occur at other extended defects, e.g., at grain boundaries. More details on surface calculations described above are presented in the Methods section.

Bulk Defects. First-principle thermodynamic calculation results (Figure 4a) indicate that bulk point defects in Cu_3N have shallow character. Cu- and N- vacancies as well as O substitutional defects in Cu_3N show shallow effective-mass-like character with the 0.1 eV transition levels. Copper interstitials in the center of the Cu_3N cube are on the boundary between the shallow and the deep character (0.3 eV transition level). Nitrogen interstitials are unstable, since there is 1.6 eV energy gain and <0.1 eV energy barrier for 2 N interstitials to recombine into a N_2 molecule in the center of the cube with no charge states in the gap. Oxygen interstitials have 1.7 eV higher formation energy than the oxygen substitutional defects, and thus are unlikely to form. The shallow defect behavior of Cu_3N (Figure 4a) contrasts with the deep defects observed in GaN (Figure 4b). The Ga vacancies are deep with (−1/0) transition level at 1.3 eV, whereas the nitrogen vacancies have a shallow character with a calculated (0/+1) transition level of 0.2 eV below the CBM.

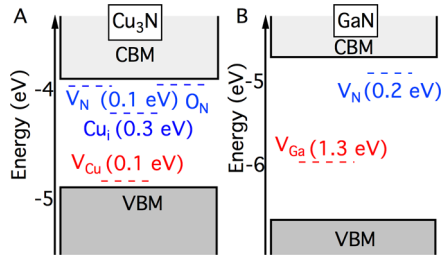

Figure 4. The first thermodynamic transition levels of native point defects in (a) Cu_3N and (b) GaN. Cu_3N has no deep point defects (a), whereas GaN does (b), in agreement with the defect tolerance argument (Abstract graphic). The origin of the energy scale in both a and b aligns with the vacuum level.

We attribute the difference in defect character between Cu_3N and GaN to the defect-tolerant electronic structure (Figure 2) of Cu_3N with the antibonding VBM. Noting that deep cation vacancies also occur in related narrow-gap nitrides, such as InN,[40] and $ZnSnN_2$,[41] the presence of only shallow defect levels

dx.doi.org/10.1021/jz5001787 | J. Phys. Chem. Lett. 2014, 5, 1117−1125

in Cu_3N is not just a trivial consequence of its narrower gap compared to GaN. Instead, it reflects the antibonding character of the Cu_3N VBM, due to which dangling bond states occur primarily as resonances inside the valence band instead of as gap states. An analogous mechanism should hold for the bonding-type character of the Cu_3N CBM (see Abstract graphic). More details on defect calculations performed here are presented in the Methods section.

Solar Energy Conversion. The results of the theoretical surface (Figure 3) and point defect (Figure 4) calculations indicate that Cu_3N due to its unusual electronic structure (Figure 2a) is a defect tolerant semiconductor with passive surfaces (Figure 3b) and shallow point defects (Figure 4b). An experimentally measurable result of shallow defects is the possibility to control the carrier type by intrinsic defects without dopants, and an implication of the unusual electronic structure is the relatively narrow band gap. Together, bipolar doping and moderate band gap make Cu_3N an attractive candidate for solar energy conversion applications, in particular polycrystalline thin film technologies that do not require single crystals or epitaxial growth. Below we present the results of experimental charge transport and optical absorption measurements that support the theoretical calculations of defect tolerance of Cu_3N, and discuss them, together with surface properties and long-term stability of this material, in the context of solar energy conversion applications.

The experimentally measured bipolar doping and the solar-matched optical absorption onset make Cu_3N a promising candidate absorber for solar cells.

Charge Transport. Experimental measurement results (Figure 5) indicate that Cu_3N can be doped with both electrons and holes. Cu_3N thin films grown under N-rich conditions have $\sim 10^{-2}$ S/cm *p*-type room-temperature conductivity with 0.1 eV activation energy. The room temperature Hall effect measurement results show 10^{16}–10^{17} cm^{-3} of free holes with μ_h = 10–1.0 $cm^2/(V\ s)$ mobility, in agreement with the measured S_h = +200 μV/K Seebeck coefficient. Cu_3N thin films deposited under Cu-rich conditions have $\sim 10^{-3}$ S/cm room-temperature conductivity with similar 0.1 eV temperature activation energy. The S_e = −40 μV/K Seebeck coefficient of these samples is indicative of *n*-type conductivity, higher concentration ($\sim 10^{17}$ cm^{-3}) and lower mobility ($\sim$0.1 $cm^2/(V\ s)$) of electrons. These experimental transport measurement results are consistent with the calculated shallow acceptors and donors (Figure 5a) in Cu_3N. The bipolar doping of Cu_3N can be viewed as a "golden mean" between Cu^{+I}-based materials (e.g., $CuInSe_2$, Cu_2S) that are often *p*-type, and nitrides (GaN, InN) that are often *n*-type, and it is quite unique since facile bipolar doping of compounds is an exception rather than a rule. We note that in Cu_2O, another Cu-based material, bipolar doping remains controversial.[42,43]

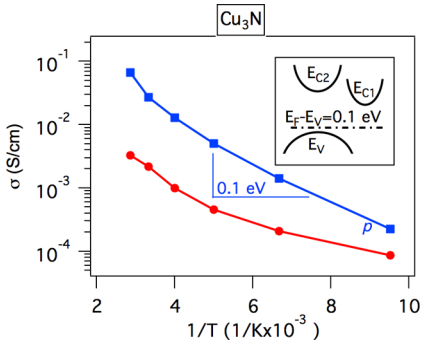

Figure 5. Temperature-dependent conductivity of *p*-type and *n*-type Cu_3N. Inset: Schematic representation of the position of the Fermi level in *p*-type Cu_3N.

The bipolar doping in Cu_3N is technologically important because it may enable formation of *p*–*n* homojunctions, the building blocks for solar cells, light-emitting diodes and other optoelectronic devices. As an example from the past, the discovery of Mg *p*-type doping in GaN led to commercial blue light-emitting devices and blue lasers based on *p*–*n* homojunctions.[44] In the area of polycrystalline thin film solar cells, the lack of bipolar doping often leads to the need for passivation of heterointerfaces, such as $CdCl_2$ "activation" of CdTe/CdS heterointerface and passivation of Cu(In,Ga)Se_2/CdS heterointerface by ordered defect compounds or Na impurities. So with regards to doping, we expect future Cu_3N photovoltaics to be similar to Si and GaAs solar cells, where formation of a *p*–*n* homojunction does not induce additional native point defects in the space charge region, and the heterointerface passivation is performed in less important parts of the solar cell, such as the front and back contacts.

Optical Absorption. The *p*-type Cu_3N thin films have absorption onset at 1.4 eV and the absorption coefficient of 10^5 cm^{-1} at 2.0 eV, according to experimental optical spectroscopy measurements (Figure 6). The theoretical optical absorption spectrum has an offset of about 0.2 eV toward higher energies, which could be explained by the temperature dependence of the band gap and/or the absence of electron–hole interaction effects in the calculated absorption spectrum.[45] The reasonably good agreement between the optical absorption measurements of the thin films and the calculated absorption coefficient (Figure 6) provides some confidence in the calculated indirect fundamental Cu_3N band gap of 1.0 eV (Table 1). The quite narrow band gaps and relatively low-energy optical absorption onsets of Cu_3N can be attributed to strong *p*–*d* repulsion in the valence band caused by small difference of the energies of Cu 3*d* and N 2*p* orbitals. In the past, the narrow band gaps of Cu-based chalcopyrites, such as $CuInSe_2$, have been attributed to (i) structural relaxation induced by the two different types of cations in the tetrahedrally bonded lattice, and to (ii) the unusual electronic structure with strong repulsion of Cu *d* and Se *p* states that shifts VBM upward compared to ZnS.[46] The measurements and calculations on the binary Cu_3N presented in this paper (Figure 6 and Table 1) show that this analysis can be extended beyond the tetrahedrally bonded ZnS and $CuInSe_2$ structures to materials with different bonding schemes and different structures such as Cu_3N and GaN (Figure 1)

The 0.4 eV difference between the experimental absorption onset and the theoretical indirect band gap of the binary Cu_3N is acceptable but not optimal for the operation of a thin film solar cell, since it may lead to the open circuit voltage deficit. As a potential solution, ternary copper nitrides, such as $CuTaN_2$ delafossite with 1.4 eV band gap, 1.5 eV absorption onset, and dumbbell N–Cu–N bonding motifs, have better light absorption properties but more anisotropic electronic structure than the binary Cu_3N.[47] $CuTaN_2$ and other ternary copper

dx.doi.org/10.1021/jz5001787 | J. Phys. Chem. Lett. 2014, 5, 1117–1125

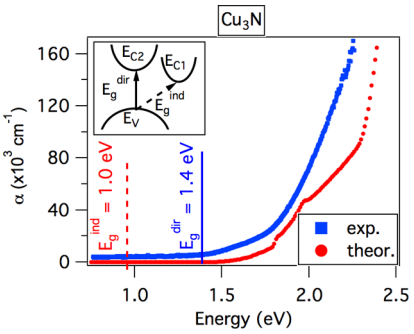

Figure 6. Optical absorption properties of *p*-type Cu_3N from experiment and theory. Inset: schematic representation of direct and indirect optical transitions in Cu_3N. The experimental absorption onset is 0.4 eV higher in energy than the theoretical band gap.

Table 2. Experimentally Measured Properties of *p*-Type Cu_3N Thin Films in Comparison with Theoretical Values Where Available[a]

property	exper.	theory
φ (eV)	5.3	–
$E_F - E_V$ (eV)	0.1	–
IP (eV)	5.4	4.9
E^{abs} (eV)	1.4	1.6
p (cm^{-3})	10^{16}–10^{17}	–
μ ($cm^2/(V\ s)$)	10–1.0	–
S ($\mu V/K$)	200	–

[a]Work function φ, energy difference between the Fermi level and the valence band $E_F - E_V$, ionization potential (IP) which is the sum of the two, optical absorption onset E^{abs}, the range of hole concentrations p and mobilities μ, and Seebeck coefficient S.

nitride absorbers are expected to retain the defect tolerant properties of the binary Cu_3N because of their comparable atomic character of the electronic band structures.[47] However, in our opinion, the examples from the real world suggest that electrical properties (which are better in Cu_3N than in $CuTaN_2$) are more important that the optical properties (which are better in $CuTaN_2$ than in Cu_3N) for photovoltaic absorber applications. As an example, the Si technology historically holds >90% market share due to facile bipolar doping (can be doped both *p*-type and *n*-type) and good carrier transport (long minority carrier lifetime), despite both nonoptimal band gap (1.1 eV instead of 1.4 eV) and weak absorption coefficient ($<10^4$ cm^{-1} below 3 eV) of this material. On the other hand, many developing thin film technologies based on materials with very strong absorption (e.g., Fe_2O_3, FeS_2) and solar-matched band gaps (Cu_2ZnSnS_4, CdTe) are still limited in their performance due to doping difficulty and poor charge carrier transport properties. Regardless of this optical/electrical trade-off, the defect tolerant charge transport properties and solar-matched band gaps that can be achieved in both binary and ternary copper nitrides such as Cu_3N and $CuTaN_2$ without the need for rare or toxic elements (such as in CdTe or PbSe) are of great importance for environmentally friendly Earth-abundant solar energy conversion applications, including both photovoltaic and photoelectrochemical cells.

Surface Properties. The results of the spectroscopic ellipsometry measurements indicate that the (001) oriented Cu_3N films when exposed to air develop a thin (<5 nm) native oxide layer, feeding into the theoretical model of Cu_3N surfaces (Figure 3a). The growth of the oxide layer on Cu_3N surfaces under ambient condition is found to be self-limiting process (samples did not change upon storing in air for over one year), which is a likely consequence of the extremely low surface energy of the partially O substituted (001) surface described above. The measured work function of the *p*-type Cu_3N surfaces is 5.3 eV, which leads to 5.4 eV estimated ionization potential given the ~0.1 eV distance from the Fermi level to the valence band (Figure 5). These measured properties of *p*-type Cu_3N along with its other physical properties are summarized in Table 2 and compared to calculated values where available. The 0.5 eV difference of the experimental estimate (5.4 eV) and the theoretical result (4.9 eV) for the ionization potential may indicate charge accumulation at Cu_3N surfaces, but further theoretical and experimental research is needed to shed more light on this possibility. Passivation of Cu_3N surfaces with a self-limiting growth of an oxide is very important for its potential photovoltaic and other optoelectronic applications. This self-terminating oxide on Cu_3N resembles that of robust TaN and TiN used for hard coatings and architectural glass applications, and contrasts with sensitive SrN_2 and Zn_3N_2 that show progressing degradation under ambient atmospheric conditions. The surface native oxide layer also makes Cu_3N similar to Si, where native SiO_2 passivation has been referred to as a "Nature's gift" to semiconductor industry, and more recently, solar cell manufacturers.

Long-Term Stability. The defect migration is an important property to consider for any semiconductor that is proposed for photovoltaic absorber applications, because it can limit the long-term operational stability of a solar cell. It is especially important for Cu-based semiconductors due to well-known high diffusivity of Cu. As an example from the past, active development of Cu_2S-based solar cell technology in the 1980s has been stopped in 1990s due to light-enhanced electromigration of copper and the resulting performance degradation of >10% efficient solar panels. This degradation was attributed to exothermic formation of copper vacancies and low defect diffusion barriers in Cu_2S structure. These issues with Cu_2S re-energized the research on much more stable $Cu(In,Ga)Se_2$ and Cu_2O photovoltaic technologies, which are currently >20% and >5% efficient respectively, with no issues related to degradation.

Our theoretical calculation results indicate that defect migration in Cu_3N is similar to that in Cu_2O and $CuInSe_2$ where it is not an issue. The lowest 1.5 eV diffusion barrier for Cu interstitials through a kick-off mechanism in Cu_3N (Figure 7, line B) is higher than the lowest 0.2 - 0.3 eV direct interstitial diffusion barrier calculated in CIGS,[48] possibly due to smaller length and higher strength of the Cu–N bond constraining the movement of atoms inside the Cu_3N lattice. The lowest energy barrier for diffusion of Cu vacancies (0.5–1.0 eV) through the indirect mechanism of formation of a Cu interstitial (Figure 7, line E) is lower than the 1.2 eV vacancy diffusion barrier in CIGS, but still higher than the interstitial diffusion barrier in this material.[49] The absence of copper migration in Cu_3N is particularly interesting given the positive formation enthalpy of this compound and its 740 K ambient-pressure[30] and 500 K low-pressure[50] limits of stability: it suggests that thermodynamic stability of a material and operational stability of a device do not exclude each other, opening a whole new class of metastable materials for solar energy conversion applications. This temperature range is likely high enough to ensure the stability of Cu_3N under typical solar cell operating conditions, yet low enough that fabrication on flexible substrates should be

dx.doi.org/10.1021/jz5001787 | J. Phys. Chem. Lett. 2014, 5, 1117–1125

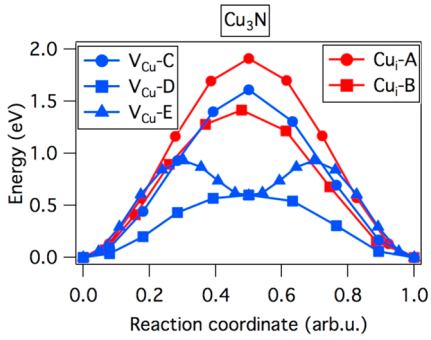

Figure 7. Theoretical defect migration energy paths through different mechanisms for copper interstitials (A - through the face of the cube; B - by kick-off of the Cu atom at the edge of the cube) and copper vacancies (C - to the opposite edge through the center of the cube; D - to the adjacent edge by passing the N atom, E - through the interstitial site in the center of the cube). The barriers in Cu_3N are at least as high as in CIGS.

possible.[51] However, the broader question of the practical use of metastable materials in applied technologies is an important topic that deserves future studies.

> Cu_3N and other materials with antibonding character of the valence band define a class of defect tolerant semiconductors for solar energy conversion applications.

As a summary, in this paper we use theoretical calculations to show that semiconductors with antibonding character of the valence band are unlikely to have deep point defect and surface states (Abstract graphic). The Cu_3N partial density of states calculations for both bulk (Figure 2) and surface (Figure 3) electronic structures support the defect tolerance in this material. The bulk point defect calculations also show no deep transition levels (Figure 4). These Cu_3N features are contrasted with surface trap states and deep character of defect transition levels in GaN semiconductor with bonding valence band character. The calculated defect tolerance of Cu_3N experimentally manifests itself in facile intrinsic bipolar doping (Figure 5). In addition, Cu_3N has the solar-matched measured 1.4 eV optical absorption onset (Figure 6) despite the calculated 1.0 eV indirect band gap (Table 1), relatively low work function (Table 2), self-limiting native surface oxide, and stability with respect to defect migration (Figure 7). All these theoretical and experimental results lead to the conclusion that the binary copper nitride Cu_3N is a promising defect tolerant light absorbers for photovoltaic and photoelectrochemical devices. The concept of defect tolerant semiconductors for solar energy conversion can be extended to a broader family of ternary copper nitrides and other materials with antibonding valence band maximum.

METHODS

Thin Film Synthesis. Copper nitride thin film samples (200−300 nm) have been grown using RF sputtering from copper target on Eagle 2000 glass substrates in a vacuum chamber with 10^{-6} Torr base pressure.[52] The RF power on the 50 mm Cu target was kept at 15−25 W and the total pressure was kept at 2×10^{-2} Torr by sourcing 10^{-2} Torr of nitrogen through a Oxford Instruments RF atomic source and balancing the rest by Ar sourced through a regular inlet. The substrate temperature of 160 °C and the target-substrate distance of 13 cm led to the N-rich growth of phase pure 00L uniaxially textured Cu_3N thin films with *p*-type conductivity. More synthesis details are reported eslwhere.[50] Polycrystalline Cu_3N with *n*-type conduction has been deposited at Cu-rich conditions with 50 W target power, 15 cm target-substrate distance, and ambient substrate temperature, under otherwise equal conditions. The synthesized Cu_3N thin films were shelf stable for over a year at ambient atmospheric conditions with natural seasonal changes in humidity.

Thin Film Characterization. Crystallographic structure and phase purity of Cu_3N thin films were determined using X-ray diffraction, the thickness was determined from X-ray fluorescence measurements verified by a profilometer, and the absorption spectra were determined from optical spectroscopy transmittance and reflectance measurements.[53] Temperature-dependent conductivity and room temperature Hall effect measurements were preformed on a commercial benchtop measurement instrument with a permanent magnet. Seebeck coefficient measurements were performed on a 4-coefficeint measurement instrument at ambient temperature. The thickness of the native oxide on Cu_3N surfaces was determined from spectroscopic ellipsometry using the Cauchy model.

Electronic Structure Calculations. The electronic structure calculations on Cu_3N and GaN were performed using the projector-augmented wave (PAW) implementation in the Vienna Ab initio Simulation Package (VASP). The Perdew−Burke−Ernzerhof (PBE) generalized gradient approximation was applied for the exchange-correlation functional in density functional theory (DFT). The DFT+U method with $U = 5$ eV was employed to for Cu-*d* orbitals in all DFT calculations. GW quasiparticle energy calculations were performed using the PAW implementations.[54] The detailed computational settings used for the GW calculations are identical to those published before,[55] including the use of an onsite-potential to account for the underbinding of Cu-*d* states in GW. The effective masses of electrons and holes were calculated by fitting the calculated density of states to the semiconductor equation[56] $N_V = 2(2\pi m_h^* k_B T/h^2)^{3/2}(E - E_0)^{1/2}$.

*Defect Calculations.*The formation enthalpies and the corresponding transition levels of defects in Cu_3N and GaN were calculated using 108-atom supercells. In order to ensure correct formation enthalpies, we applied potential alignment and finite size corrections,[57] as well as GW-derived band edge shifts[58] and fitted elemental-phase reference energies,[59] which in turn lead to more accurate results for the reported transition levels. The defect states of gallium vacancy in GaN have been calculated using the ab initio polaron theory,[60] with the parameter $\lambda = 3.1$ eV determined in that study for Mg dopants. Similar approach has been applied to verify that the Cu_3N defects are have shallow character. Diffusion barriers were calculated using the Climbing Image Nudged Elastic Band method[61] together with the PBE+U Hamiltonian: all ionic positions were allowed to be relaxed, and the volume was kept constant. Supercell size effect in the value of the diffusion barrier was found to be negligible.

Surface Calculations. We modeled Cu_3N and GaN surfaces using the standard approach described in greater detail elsewhere.[62] The periodic supercell slab geometry was

dx.doi.org/10.1021/jz5001787 | J. Phys. Chem. Lett. 2014, 5, 1117−1125

employed with symmetric slabs constructed from the fully relaxed bulk unit cells. Two quantities, the surface energies and the average electrostatic potentials (i.e., surface dependent material/vacuum potential step) were converged both with respect to the slab thickness and the length of the vacuum region. Surface orientation-dependent ionization potentials and electron affinities are then computed by combining the bulk GW electronic structure and the material/vacuum potential steps from DFT+U surface calculations. For the self-consistent band gap corrected calculation of the surface electronic structure, we used an extension of the nonlocal external potential method,[63] where we determined two parameters per atom type and angular momentum.

AUTHOR INFORMATION

Corresponding Author

*Mailing address: National Renewable Energy Laboratory, 15013 Denver West Parkway, Golden, CO 80401-3305 USA. Phone: 303-384-6467. Fax: 303-384-643. E-mail: Andriy.Zakutayev@nrel.gov.

Notes

The authors declare no competing financial interest.

Biographies

Andriy Zakutayev is a scientist at National Renewable Energy Laboratory (NREL) working on development of next-generation solar energy conversion technologies using high-throughput combinatorial thin film methods in close coupling with first-principles calculations. Andriy received his Ph.D. in Physics from Oregon State University where he studied mixed-anion *p*-type transparent conductors. https://sites.google.com/site/andriyzakutayev

Christopher M. Caskey is a Ph.D. candidate at Colorado School of Mines (CSM) preforming research at NREL on combinatorial synthesis and characterization of nitride thin films. Prior to joining CSM, he worked in analytical chemistry and failure analysis in Seattle, Washington. He received his B.S. in Chemistry from The University of Arizona in 2008.

Angela Fioretti is a joint Ph.D. student in Materials Science at Colorado School of Mines and the National Renewable Energy Laboratory (NREL). Her thesis work studies the optoelectronic properties of novel nitride semiconductors for application as solar absorbers. Her technical specialty is reactive RF-magnetron sputtering of thin film materials.

David S. Ginley is a research fellow at NREL with experience in a broad range of functional materials and renewable energy technologies. Prior to joining NREL, he worked at Sandia National Laboratories as a manager of the Advanced Materials. Dr. Ginley received his Ph.D. in Inorganic Chemistry from MIT.

Julien Vidal is a researcher at EDF Lab, France, investigating the electrical and optical properties of photovoltaic materials by means of ab initio calculations. Julien received his Ph.D. in Physics from Ecole Polytechnique, France, where he studies the electronic structure of $CuInS_2$ by means of Many Body Perturbation Theory.

Vladan Stevanovic is a Research Assistant Professor with joint appointment between the Department of Physics, Colorado School of Mines, and the National Renewable Energy Laboratory. His field of expertise is theoretical/computational solid state physics and materials science. Vladan received his Ph.D. from EPFL, Switzerland, where he studied catalytic properties of oxide supported transition metal clusters.

Eric Tea is a postdoctoral fellow at the Institute for Research and Development for Photovoltaic Energy (IRDEP), France, where he studies electronic properties of III−V compounds for photovoltaic application. He obtained his Ph.D. in Physics at Paris-Sud University where he modeled Hot Carrier Solar Cells by means of Ensemble Monte Carlo methods.

Stephan Lany is a theoretical/computational materials scientist with research interests in electronic structure calculations, semiconductor physics, defects and impurities, photovoltaic materials, and materials by design. He received his Ph.D. in Physics in 2002 from the Universität des Saarlandes, and is presently a Senior Scientist at the National Renewable Energy Laboratory.

ACKNOWLEDGMENTS

This research is supported by the U.S. Department of Energy, office of Energy Efficiency and Renewable Energy, as a part of the "Ternary Copper Nitride Absorbers" Next Generation PV II project within the SunShot initiative under Contract No. DE-AC36-08GO28308 to NREL.

REFERENCES

(1) Rockett, A. A. Current Status and Opportunities in Chalcopyrite Solar Cells. *Curr. Opin. Solid State Mater. Sci.* **2010**, *14*, 143−148.

(2) Friedman, D. J. Progress and Challenges for Next-Generation High-Efficiency Multijunction Solar Cells. *Curr. Opin. Solid State Mater. Sci.* **2010**, *14*, 131−138.

(3) Wadia, C.; Alivisatos, A. P.; Kammen, D. M. Materials Availability Expands the Opportunity for Large-Scale Photovoltaics Deployment. *Environ. Sci. Technol.* **2009**, *43*, 2072−2077.

(4) Rühle, S.; Anderson, A. Y.; Barad, H.-N.; Kupfer, B.; Bouhadana, Y.; Rosh-Hodesh, E.; Zaban, A. All-Oxide Photovoltaics. *J. Phys. Chem. Lett.* **2012**, *3*, 3755−3764.

(5) Maeda, K.; Domen, K. Photocatalytic Water Splitting, Recent Progress and Future Challenges. *J. Phys. Chem. Lett.* **2010**, *1*, 2655−2661.

(6) Rashkeev, S. N.; Limpijumnong, S.; Lambrecht, W. R. Second-Harmonic Generation and Birefringence of Some Ternary Pnictide Semiconductors. *Phys. Rev. B* **1999**, *59*, 2737.

(7) Lahourcade, L.; Coronel, N. C.; Delaney, K. T.; Shukla, S. K.; Spaldin, N. A.; Atwater, H. A. Structural and Optoelectronic Characterization of RF Sputtered $ZnSnN_2$. *Adv. Mater.* **2013**, *25*, 2562−2566.

(8) Scanlon, D. O.; Walsh, A. Bandgap Engineering of $ZnSnP_2$ for High-Efficiency Solar Cells. *Appl. Phys. Lett.* **2012**, *100*, 251911−251911.

(9) Ponce, F. A.; Bour, D. P. Nitride-Based Semiconductors for Blue and Green Light-Emitting Devices. *Nature* **1997**, *386*, 351−359.

(10) Wu, J.; Walukiewicz, W.; Yu, K. M.; Shan, W.; Ager Iii, J. W.; Haller, E. E.; Lu, H.; Schaff, W. H.; Metzger, W. K.; Kurtz, S. Superior Radiation Resistance of InGaN Alloys, Full-Solar-Spectrum Photovoltaic Material System. *J. Appl. Phys.* **2003**, *94*, 6477.

(11) Meyer, B. K.; Polity, A.; Reppin, D.; Becker, M.; Hering, P.; Klar, P. J.; Sander, Th.; Reindl, C.; Benz, J.; Eickhoff, M. Binary Copper Oxide Semiconductors, from Materials Towards Devices. *Phys. Status Solidi B* **2012**, *249*, 1487−1509.

(12) Tate, J.; Ju, H. L.; Moon, J. C.; Zakutayev, A.; Richard, A. P.; Russell, J.; McIntyre, D. H. Origin of P-Type Conduction in Single-Crystal $CuAlO_2$. *Phys. Rev. B* **2009**, *80*, 165206.

(13) Scanlon, D. O.; Watson, G. W. Conductivity Limits in $CuAlO_2$ from Screened-Hybrid Density Functional Theory. *J. Phys. Chem. Lett.* **2010**, *1*, 3195−3199.

(14) Zawadzki, P.; Baranowski, L. L.; Peng, H.; Toberer, E. S.; Ginley, D. S.; Tumas, W.; Zakutayev, A.; Lany, S. Evaluation of Photovoltaic Materials Within the Cu−Sn−S Family. *Appl. Phys. Lett.* **2013**, *103*, 253902.

(15) Yu, L.; Kokenyesi, R. S.; Keszler, D. A.; Zunger, A. Inverse Design of High Absorption Thin-Film Photovoltaic Materials. *Adv. Eng. Mater.* **2013**, *3*, 43−48.
(16) Tate, J.; Newhouse, P. F.; Kykyneshi, R.; Hersh, P. A.; Kinney, J.; McIntyre, D. H.; Keszler, D. A. Chalcogen-Based Transparent Conductors. *Thin Solid Films* **2008**, *516*, 5795−5799.
(17) Ueda, K.; Hiramatsu, H.; Hirano, M.; Kamiya, T.; Hosono, H. Wide-Gap Layered Oxychalcogenide Semiconductors, Materials, Electronic Structures and Optoelectronic Properties. *Thin Solid Films* **2006**, *496*, 8−15.
(18) Minami, T.; Nishi, Y.; Miyata, T. High-Efficiency Cu_2O-Based Heterojunction Solar Cells Fabricated Using a Ga_2O_3 Thin Film as N-Type Layer. *Appl. Phys. Exp.* **2013**, *6*, 044101.
(19) Lee, Y. S.; Heo, J.; Siah, S. C.; Mailoa, J. P.; Brandt, R. E.; Kim, S. B.; Gordon, R. G.; Buonassisi, T. Ultrathin Amorphous Zinc-Tin-Oxide Buffer Layer for Enhancing Heterojunction Interface Quality in Metal-Oxide Solar Cells. *Energy Environ. Sci.* **2013**, *6*, 2112−2118.
(20) Paracchino, A.; Laporte, V.; Sivula, K.; Grätzel, M.; Thimsen, E. Highly Active Oxide Photocathode for Photoelectrochemical Water Reduction. *Nat. Mater.* **2011**, *10*, 456−461.
(21) Joshi, U. A.; Maggard, P. A. $CuNb_3O_8$: A P-Type Semiconducting Metal Oxide Photoelectrode. *J. Phys. Chem. Lett.* **2012**, *3*, 1577−1581.
(22) Zakutayev, A.; Newhouse, P. F.; Kykyneshi, R.; Hersh, P. A.; Keszler, D. A.; Tate, J. Pulsed Laser Deposition of BiCuOSe Thin Films. *Appl. Phys. A: Mater. Sci. Process.* **2011**, *102*, 485−492.
(23) Pei, Y. L.; He, J.; Li, J. F.; Li, F.; Liu, Q.; Pan, W.; Barreteau, C.; Berardan, D.; Dragoe, N.; Zhao, L. D. High Thermoelectric Performance of Oxyselenides: Intrinsically Low Thermal Conductivity of Ca-Doped BiCuSeO. *NPG Asia Mater.* **2013**, *5*, e47.
(24) Zakutayev, A.; Kykyneshi, R.; Schneider, G.; McIntyre, D. H.; Tate, J. Electronic Structure and Excitonic Absorption in BaCuChF (Ch = S, Se, and Te). *Phys. Rev. B* **2010**, *81*, 155103.
(25) Zakutayev, A.; McIntyre, D. H.; Schneider, G.; Kykyneshi, R.; Keszler, D. A.; Park, C.-H.; Tate, J. Tunable Properties of Wide-Band Gap P-type $BaCu(Ch_{1-x}Ch_x')$ F (Ch = S, Se, Te) Thin-Film Solid Solutions. *Thin Solid Films* **2010**, *518*, 5494−5500.
(26) Matsuzaki, K.; Nomura, K.; Yanagi, H.; Kamiya, T.; Hirano, M.; Hosono, H. Epitaxial Growth of High Mobility Cu_2O Thin Films and Application to P-Channel Thin Film Transistor. *Appl. Phys. Lett.* **2008**, *93*, 202107.
(27) Nandy, S.; Banerjee, A.; Fortunato, E.; Martins, R. A Review on Cu_2O and Cu^I-Based p-Type Semiconducting Transparent Oxide Materials, Promising Candidates for New Generation Oxide Based Electronics. *Rev. Adv. Sci. Eng.* **2013**, *2*, 273−304.
(28) Maya, L. Deposition of Crystalline Binary Nitride Films of Tin, Copper, and Nickel by Reactive Sputtering. *J. Vac. Sci. Technol. A* **1993**, *11*, 604−608.
(29) Soto, G.; Diaz, J. A.; De La Cruz, W. Copper Nitride Films Produced by Reactive Pulsed Laser Deposition. *Mater. Lett.* **2003**, *57*, 4130−4133.
(30) Hahn, U.; Weber, W. Electronic Structure and Chemical-Bonding Mechanism of Cu_3N, Cu_3NPd, and Related Cu (I) Compounds. *Phys. Rev. B* **1996**, *53*, 12684.
(31) Modin, A.; Kvashnina, K. O.; Butorin, S. M.; Werme, L.; Nordgren, J.; Arapan, S.; Ahuja, R.; Ottosson, M. Electronic Structure of Cu_3N Films Studied by Soft X-ray Spectroscopy. *J. Phys.: Condens. Matter* **2008**, *20*, 235212.
(32) Borsa, D. M.; Boerma, D. O. Growth, Structural and Optical Properties of Cu_3N Films. *Surf. Sci.* **2004**, *548*, 95−105.
(33) Liu, Z. Q. Thermal Stability of Copper Nitride Films Prepared by RF Magnetron Sputtering. *Thin Solid Films* **1998**, *325*, 55−59.
(34) Asano, M.; Kazuo, U.; Akira, T. Cu_3N Thin Film for a New Light Recording Media. *Jpn. J. Appl. Phys.* **1990**, *29*, 1985.
(35) Pereira, N.; Dupont, L.; Tarascon, J. M.; Klein, L. C.; Amatucci, G. G. Electrochemistry of Cu_3N with Lithium A Complex System with Parallel Processes. *J. Electrochem. Soc.* **2003**, *150*, A1273−A1280.
(36) Segev, D.; Van de Walle, C. G. Origins of Fermi-Level Pinning on GaN and InN Polar and Nonpolar Surfaces. *Europhys. Lett.* **2006**, *76*, 305.
(37) Himmerlich, M.; Lymperakis, L.; Gutt, R.; Lorenz, P.; Neugebauer, J.; Krischok, S. GaN (0001) Surface States, Experimental and Theoretical Fingerprints to Identify Surface Reconstructions. *Phys. Rev. B* **2013**, *88*, 125304.
(38) Martinez, G. L.; Curiel, M. R.; Skromme, B. J.; Molnar, R. J. Surface Recombination and Sulfide Passivation of GaN. *J. Electron. Mater.* **2000**, *29*, 325−331.
(39) Gila, B. P.; Ren, F.; Abernathy, C. R. Novel Insulators for Gate Dielectrics and Surface Passivation of GaN-based Electronic Devices. *Mater. Sci. Eng., R* **2004**, *44*, 151−184.
(40) Janotti, A.; Lyons, J. L.; Van de Walle, C. G. Hybrid Functional Calculations of Native Point Defects in InN. *Phys. Status Solidi A* **2012**, *209*, 65−70.
(41) Chen, S.; Narang, P.; Atwater, H. A.; Wang, L. W. Phase Stability and Defect Physics of a Ternary $ZnSnN_2$ Semiconductor, First Principles Insights. *Adv. Mater.* **2013**, *26*, 311.
(42) McShane, C. M.; Siripala, W. P.; Choi, K.-S. Effect of Junction Morphology on the Performance of Polycrystalline Cu_2O Homojunction Solar Cells. *J. Phys. Chem. Lett.* **2010**, *1*, 2666−2670.
(43) Scanlon, D. O.; Watson, G. W. Undoped n-Type Cu_2O: Fact or Fiction? *J. Phys. Chem. Lett.* **2010**, *1*, 2582−2585.
(44) Amano, H.; Kito, M.; Hiramatsu, K.; Akasaki, I. P-type Conduction in Mg-Doped GaN Treated with Low-Energy Electron Beam Irradiation (LEEBI). *Jpn. J. Appl. Phys.* **1989**, *28*, L2112−L2114.
(45) Vidal, J.; Lany, S.; dAvezac, M.; Zunger, A.; Zakutayev, A.; Francis, J.; Tate, J. Band-Structure, Optical Properties, and Defect Physics of the Photovoltaic Semiconductor SnS. *Appl. Phys. Lett.* **2012**, *100*, 032104−032104.
(46) Jaffe, J. E.; Zunger, A. Theory of the Band-gap Anomaly in ABC_2 Chalcopyrite Semiconductors. *Phys. Rev. B* **1984**, *29*, 1882.
(47) Yang, M.; Zakutayev, A.; Vidal, J.; Zhang, X.; Ginley, D. S.; DiSalvo, F. J. Strong Optical Absorption in $CuTaN_2$ Nitride Delafossite. *Energy Environ. Sci.* **2013**, *6*, 2994−2999.
(48) Pohl, J.; Klein, A.; Albe, K. Role of Copper Interstitials in $CuInSe_2$, First-Principles Calculations. *Phys. Rev. B* **2011**, *84*, 121201.
(49) Pohl, J.; Albe, K. Thermodynamics and Kinetics of the Copper Vacancy in $CuInSe_2$, $CuGaSe_2$, $CuInS_2$, and $CuGaS_2$ from Screened-Exchange Hybrid Density Functional Theory. *J. Appl. Phys.* **2010**, *108*, 023509.
(50) Caskey, C. M.; Richards, R. M.; Ginley, D. S.; Zakutayev, A. Synthesis and Properties of Copper Nitride, a Metastable Semiconductor. *Mater. Horiz.* Submitted for publication, 2014
(51) Chirila, A.; Buecheler, S.; Pianezzi, F.; Bloesch, P.; Gretener, C.; Uhl, A. R.; Fella, C.; Kranz, L.; Perrenoud, J.; Seyrling, S.; et al. Highly efficient $Cu(In,Ga)Se_2$ Solar Cells Grown on Flexible Polymer Films. *Nat. Mater.* **2011**, *10*, 857.
(52) Zakutayev, A.; Perkins, J. D.; Parilla, P. A.; Widjonarko, N. E.; Sigdel, A. K.; Berry, J. J.; Ginley, D. S. Zn−Ni−Co−O Wide-Band-Gap P-type Conductive Oxides with High Work Functions. *MRS Commun.* **2011**, *1*, 23−26.
(53) Zakutayev, A.; Paudel, T. R.; Ndione, P. F.; Perkins, J. D.; Lany, S.; Zunger, A.; Ginley, D. S. Cation Off-Stoichiometry Leads to High p-Type Conductivity and Enhanced Transparency in Co_2ZnO_4 and Co_2NiO_2 Thin Films. *Phys. Rev. B* **2012**, *85*, 085204.
(54) Shishkin, M.; Kresse, G. Implementation and Performance of the Frequency-Dependent GW Method within the PAW Framework. *Phys. Rev. B* **2006**, *74*, 035101.
(55) Lany, S. Band-Structure Calculations for the 3d Transition Metal Oxides in GW. *Phys. Rev. B* **2013**, *87*, 085112.
(56) Sze, S. M.; Ng, K. K. *Physics of Semiconductor Devices*; John Wiley & Sons: Hoboken, NJ, 2006
(57) Lany, S.; Zunger, A. Assessment of Correction Methods for the Band-gap Problem and for Finite-size Effects in Supercell Defect Calculations, Case Studies for ZnO and GaAs. *Phys. Rev. B* **2008**, *78*, 235104.

(58) Peng, H.; Scanlon, D. O.; Stevanovic, V.; Vidal, J.; Watson, G. W.; Lany, S. Convergence of Density and Hybrid Functional Defect Calculations for Compound Semiconductors. *Phys. Rev. B* **2013**, *88*, 115201.
(59) Lany, S. Semiconductor Thermochemistry in Density Functional Calculations. *Phys. Rev. B* **2008**, *78*, 245207.
(60) Lany, S. Predicting Polaronic Defect States by Means of Generalized Koopmans Density Functional Calculations. *Phys. Status Solidi B* **2011**, *248*, 1052−1060.
(61) Henkelman, G.; Uberuaga, B. P.; Jónsson, H. A Climbing Image Nudged Elastic Band Method for Finding Saddle Points and Minimum Energy Paths. *J. Chem. Phys.* **2000**, *113*, 9901.
(62) Stevanovic, V.; Lany, S.; Ginley, D. S.; Tumas, W.; Zunger, A. Assessing Capability of Semiconductors to Split Water Using Ionization Potentials and Electron Affinities Only. *Phys. Chem. Chem. Phys.* **2014**, *16*, 3706.
(63) Lany, S.; Raebiger, H.; Zunger, A. Magnetic Interactions of Cr−Cr and Co−Co Impurity Pairs in ZnO Within a Band-Gap Corrected Density Functional Approach. *Phys. Rev. B* **2008**, *77*, 241201.